

Fast time variations of supernova neutrino signals from 3-dimensional models

Tina Lund,¹ Annop Wongwathanarat,² Hans-Thomas Janka,² Ewald Müller,² and Georg Raffelt³

¹*Department of Physics, North Carolina State University, 2401 Stinson Drive, Raleigh, NC 27607, USA*

²*Max-Planck-Institut für Astrophysik, Karl-Schwarzschild-Str. 1, 85748 Garching, Germany*

³*Max-Planck-Institut für Physik (Werner-Heisenberg-Institut), Föhringer Ring 6, 80805 München, Germany*

(Dated: 31 July 2012)

We study supernova neutrino flux variations in the IceCube detector, using 3D models based on a simplified neutrino transport scheme. The hemispherically integrated neutrino emission shows significantly smaller variations compared with our previous study of 2D models, largely because of the reduced SASI activity in this set of 3D models which we interpret as a pessimistic extreme. For the studied cases, intrinsic flux variations up to about 100 Hz frequencies could still be detected in a supernova closer than about 2 kpc.

PACS numbers: 14.60.Pq, 97.60.Bw

I. INTRODUCTION

Measuring the neutrino signal from a future galactic core-collapse supernova (SN) will provide valuable information about the conditions in the collapsing stellar core and in the forming compact remnant. In particular neutrinos and gravitational waves will serve as direct probes of the explosion mechanism. While neutrino energy deposition is most widely favored as the trigger and energy supply of the SN blast wave [1], the success of this mechanism in iron-core SNe turns out to be tightly linked to the development of violent nonradial mass flows in the layer behind the stalled bounce shock (see Ref. [2] for a recent review).

Multi-dimensional hydrodynamical models have shown that nonradial gas motions naturally grow from small initial perturbations in the neutrino-heated, shocked accretion flow because of convective instability [3] and the standing accretion shock instability (SASI) [4]. Violent, quasi-periodic expansion and contraction (“sloshing”) of the shock can lead to considerable variation of the mass accretion rate to the proto-neutron star (PNS). In axisymmetric (2D) models, where the sloshing motions are artificially constrained to proceed along the symmetry axis, these variations and the associated compression of the PNS “surface” layer can produce fluctuations of the observable (hemispherically integrated) neutrino emission of more than 10% in luminosity and of 0.5–1 MeV in the mean spectral energy; the polar emission variations are even larger [5]. Such large variations of the neutrino emission would be easily detectable for a galactic SN with IceCube or future megaton-class instruments, and the presence of Fourier components with frequencies of tens of Hz up to 200–300 Hz would provide important information on the SN core dynamics prior to the onset of the explosion [6, 7]. They could also allow one to constrain neutrino masses [8] and to probe neutrino propagation over cosmic distances [9].

Because of the directing effect of the symmetry axis the SASI sloshing motions appear particularly strongly in 2D core-collapse simulations, independently of whether de-

tailed neutrino transport [5, 7, 10–13], simplified neutrino cooling and heating terms [14–16], a schematic cooling prescription, or an outflow boundary at the bottom of the otherwise adiabatic accretion flow [4, 17] is used.

In three-dimensional (3D) models, low-order multipole SASI sloshing motions have so far been observed only with considerably reduced amplitudes and stochastically changing direction [18] or no clear signatures of SASI sloshing activity were seen [19–22]. Indeed, it has been claimed that buoyancy-driven convection dominates post-shock turbulence [23] and the SASI is “at most a minor feature of SN dynamics” [22]. Such conclusions, however, should be taken with caution. They rely on small sets of 3D models with idealized setups, e.g., only including simple neutrino heating and cooling terms but without detailed neutrino transport and its feedback on the PNS evolution. They therefore do not explore the important influence of PNS contraction driven by energy and lepton losses through neutrino emission as well as progenitor-specific differences, both of which were shown to be able to fundamentally change the dynamics of the postshock accretion flow [2, 10, 12]. Moreover, the conditions for developing SASI spiral modes [17, 24, 25] in SN cores are neither fully understood nor satisfactorily investigated. The growth timescale of such modes can be strongly reduced by even small amounts of rotation in the collapsing stellar matter [26] and their appearance is observed in experimental analogies [27]. Low-mode asymmetries, which are much bigger than seen in present, first 3D simulations and which impose quasi-periodic, large-amplitude variability on the PNS neutrino emission, can therefore not be excluded.

We here take the pessimistic point of view and apply our previous analysis of 2D models [6] to several recent 3D explosion calculations which show only a low level of SASI activity and no signs of long-lasting sloshing motions [20], in contrast to the 2D simulations of Marek, Janka and Müller [5] evaluated by Lund et al. [6]. Nevertheless, even for such unfavorable conditions our results suggest that the modulation of the neutrino emission below about 100 Hz will be detectable with IceCube for a galactic SN up to a distance of 2 kpc.

The outline of our paper is as follows. In Sec. II we summarize essential information about the simulated models and the expected signal rates in IceCube. In Sect. III we present the power spectra that can be deduced from a measurement and discuss their meaning. In Sect. IV we explore the detectability of the intrinsic neutrino signal variations in competition with the shot noise of the IceCube measurement. Conclusions will be given in Sec. V.

II. SUPERNOVA MODELS

A. Investigated models

The 3D simulations providing the neutrino luminosities and mean spectral energies for our analysis are models W15-4, L15-3, and N20-2 from the larger set of explosion models published in [20], where also more details about the numerical methods and setup can be found. These simulations are based on three nonrotating progenitors, the $15 M_{\odot}$ model s15s7b2 of Woosley and Weaver [28], a $15 M_{\odot}$ star computed by Limongi et al. [29], and a $20 M_{\odot}$ model provided by Shigeyama and Nomoto [30], respectively. In Table I some characteristic properties of our three investigated explosion models are listed.

The 3D explosion modeling was performed with the explicit, finite-volume, Eulerian, multi-fluid hydrodynamics code PROMETHEUS [31–33]. An axis-free, overlapping “Yin-Yang” grid technique in spherical polar coordinates was used [34, 35], employing an angular resolution of 2° over the full 4π solid angle. A combined linearly and logarithmically spaced grid with 400 radial zones allowed for a minimum resolution of 0.3 km between the inner grid boundary and the outer boundary at 18,000 km. The high-density core of the PNS above roughly 10 times the neutrinospheric density was excised and replaced by a gravitating point mass at the coordinate center and an inner grid boundary, whose retraction from 60–80 km shortly after bounce to 20–30 km after about 1 s was prescribed to mimic the shrinking of the PNS due to energy and lepton number losses by neutrino emission.

TABLE I. Properties of our models.

Model	L15-3	W15-4	N20-2
Simulation end time [ms]	1414	1315	1314
Explosion time [ms]	477	272	265
Analysis interval length τ [ms]	500	300	350
N_{bins}	500	300	350
N_{events} [10^7] at 1 kpc	2.89	1.72	2.50
Frequency resolution δf [Hz]	2.0	3.3	2.9
P_0 [10^9] at 1 kpc	3.34	3.29	5.10
P_{comb} at 1 kpc	346	573	612
P_{bkgd}	8.0	13.4	11.5
P_{99} at 2 kpc	399	660	705

Explosions of the models with chosen energies were initiated by picking suitable values of the (time-dependent) neutrino luminosities imposed spherically symmetrically at the inner grid boundary. On the computational grid the transport and matter interactions of neutrinos of all flavors were approximated by the grey (non-spectral) transport scheme described in Scheck et al. [36], solving the 1D (spherically symmetric) transport equation in each angular grid bin independently. This “ray-by-ray” approximation allowed for taking into account directional variations of the neutrino fluxes.

With this setup the neutrino-driven explosions could be followed until well beyond one second after bounce, at which time the explosion energy was essentially saturated. Starting from initial random seed perturbations (imposed as cell-to-cell variations on the level of 0.1% of the radial velocity), large-scale asymmetries in the accretion flow between the stalled shock and PNS “surface” developed (due to the action of convective instability and the SASI) and supported the onset of the explosion. Asymmetric accretion onto the nascent neutron star (NS) continued considerably longer. During the accretion phase a sizable part of the ν_e and $\bar{\nu}_e$ emission (around 50%) was produced in the hot, settling accretion layer between the inner grid boundary and the gain radius, which bounds the neutrino-heating layer from below.

The direction-dependent neutrino transport results were used to deduce time-dependent information on the observable neutrino luminosities for our models as described in Sect. 3 of [20]. To this end the emission was integrated over the hemisphere seen by an observer from a certain direction, approximately accounting for the limb darkening effect that is associated with a non-isotropic angular distribution of the neutrinos in the layer of neutrino-matter decoupling. For the analysis in this paper we chose five viewing directions, which are orthogonal to each other and can be considered as representative, because the neutrino emission in the (nonrotating) 3D models does not possess any preferred direction. This can be verified from Fig. 1, where the expected IceCube detection rates show similar time dependence and differ only in details for all investigated viewing angles. In addition to the observable luminosities the grey neutrino transport also provides the mean energies of the radiated neutrinos as the ratio of neutrino energy flux to neutrino number flux.

B. Neutrino emission from SN cores

The count rates displayed in Fig. 1 reflect the familiar behavior of the $\bar{\nu}_e$ emission from a SN core. While the mean neutrino energies increase with time mostly monotonically after bounce, the luminosities exhibit a steep rise over a timescale of typically 100 ms, followed by a broad accretion hump of 400–600 ms, whose length depends on the duration of the postbounce accretion

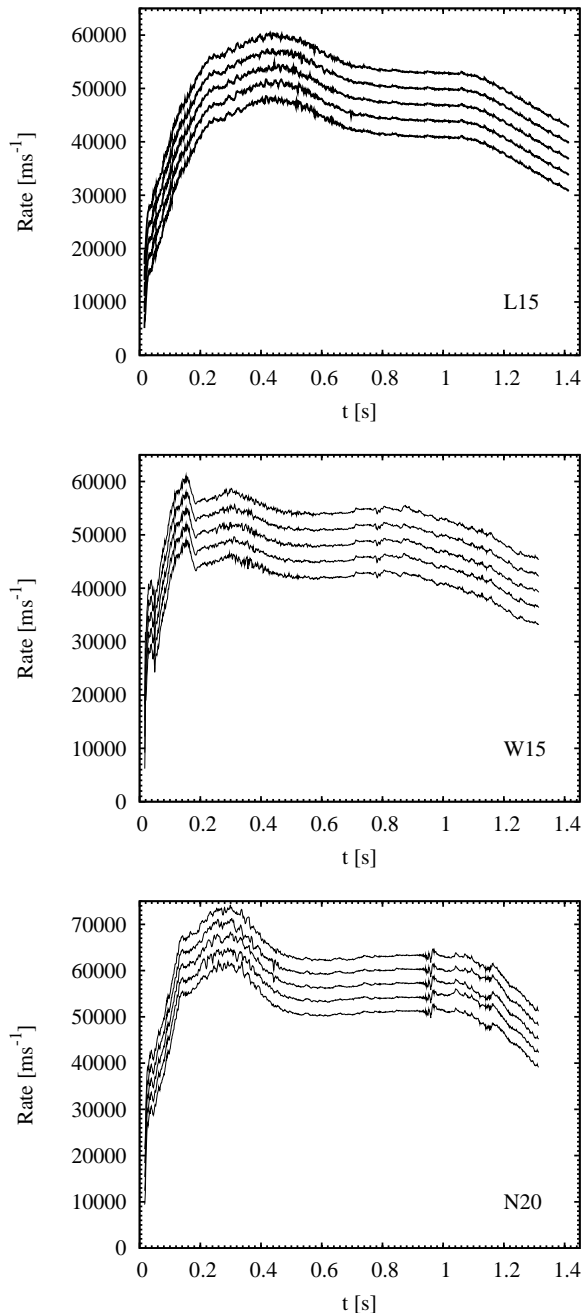


FIG. 1. Event rates in IceCube from our 3D models for a SN at 1 kpc. The models are L15, W15 and N20 from top to bottom as indicated. The rates are hemispheric flux integrals for the five viewing directions, with hemisphere 5 on top and other curves offset consecutively by -3000 units.

phase, and finally, after the onset of the explosion, the luminosities make a transition to a continuous decline, which marks the beginning of the PNS cooling evolution (see also Fig. 9 in [20]). Besides rapid fluctuations on timescales between several and tens of ms and maximum amplitudes on the 5% level, the event rates also show modulations on longer timescales. These are connected

to variations of the mass infall rate to the shock, which is determined by the density structure of the collapsing progenitor core. In particular the W15 model reveals the effects of sharp composition-shell interfaces. When the latter fall through the shock, the mass accretion rate drops rapidly and the accretion luminosity follows this behavior with a short delay (the most prominent of these features is seen in the W15 model between 180 and 200 ms). At late times ($t \gtrsim 800$ – 1000 ms) quasiperiodic, low-level variability is associated with convective activity close to the neutrinospheric layer inside the PNS, and aperiodic, stronger outbursts are a consequence of episodic, asymmetric fallback of gas to the PNS.

The fast variability with frequencies between ~ 30 Hz and ~ 200 Hz during the phase of massive accretion is caused by large-scale, intermittent accretion funnels, which carry infalling matter from the SN shock front to the newly formed NS. These asymmetrically distributed, strongly time-dependent accretion streams are associated with the convective overturn in the neutrino-heating layer and can be influenced by SASI motions of the shock and postshock mass distribution. The corresponding activity between PNS and shock becomes particularly strong after 100–200 ms of postbounce evolution in all investigated models. At this time neutrino-flux variations develop on different angular scales, but soon the emission asymmetry becomes dominated by low spherical harmonics modes ($\ell = 1$ – 4). For hundreds of milliseconds, well beyond the onset of the explosions, the neutrino emission exhibits strong intensity maxima where a few large, well-localized accretion downdrafts impact the neutrinospheric layer (for details, see [20]). Because the location of these hot spots can be relatively stationary (especially when the shock expansion has set in and the convective bubble pattern begins to freeze out), the luminosity variations visible for an observer from a certain direction carry information about the typical coherence timescale of the accretion flows feeding the asymmetric emission. This coherence timescale is roughly set by the infall time of matter through the accretion funnels, $\sim (R_s - R_{\text{NS}})/|v_r|$, and is estimated to be tens of milliseconds for representative values of the shock radius, R_s , PNS radius, R_{NS} , and radial velocity, v_r .

C. Neutrino signal in IceCube

As in our previous study [6], we consider the neutrino signal in IceCube because it produces the largest event statistics of all operating SN neutrino detectors. The grey neutrino transport approximation employed in our models only provides average neutrino energies without detailed spectral information and we assume thermal distributions. Following our previous estimate, the expected

signal rate then is

$$R_{\bar{\nu}_e} = 153 \text{ ms}^{-1} \frac{L_{\bar{\nu}_e}}{10^{52} \text{ erg s}^{-1}} \left(\frac{10 \text{ kpc}}{D} \right)^2 \left(\frac{E_{\text{av}}}{12 \text{ MeV}} \right)^2. \quad (1)$$

Even without a SN signal, the detector produces a background (bkgd) event rate of approximately

$$R_{\text{bkgd}} = 1340 \text{ ms}^{-1}. \quad (2)$$

It must be added to the SN induced signal to obtain the total event rate R_{tot} . We display the expected counting rates for an assumed distance of 1 kpc in Fig. 1 for the five observation directions mentioned earlier.

Numerical models in 2D showed strong dipolar and quadrupolar motions [5, 10] that imparted excursions in the neutrino luminosity of up to 30% and up to 15% in the mean neutrino energy. The resulting event-rate fluctuations were almost up to 20%. This meant that a detailed power spectrum could be obtained for a SN out to a distance of 10 kpc [6]. In the case of our 3D models, the SASI and convective flows are much less coherent in space. Consequently, the amplitudes of variations in the neutrino luminosities and mean energies are considerably smaller. This reduction reflects in the event rates shown in Fig. 1, where the fluctuations amount to only a few percent. We therefore focus our analysis on a fiducial SN distance of 1 kpc instead of the previously used 10 kpc.

The sharp dips in the event rate seen particularly for the W15 model are caused by burning-shell interfaces falling through the accretion shock. The corresponding drops in density reduce the accretion rate and the neutrino emission. The effect of shell interfaces was clearly visible in spherical simulations but appeared to be obscured or dwarfed in 2D by the fairly large SASI-induced emission fluctuations. In 3D, where the SASI effects are smaller, the shell interfaces become visible once again.

In contrast to the axisymmetric 2D simulations, there is no preferred spatial direction in 3D (if rotation is absent in the stellar core), and the event rates in all viewing directions are very similar (see Fig. 1). In the following we will always use “hemisphere 5” as our benchmark case.

We focus our analysis on the accretion phase where the neutrino signal and its variations are largest. On the other hand, convective overturn and SASI activity take some time to develop. For an analysis interval we therefore begin at 100 ms post bounce until somewhat after the explosion takes off. Specifically, we will use time intervals $\tau = 300$ ms (W15), 350 ms (N20) and 500 ms (L15) as listed in Table I.

III. POWER SPECTRA

We show the power spectra of our three benchmark cases in Fig. 2, i.e. the “hemisphere 5” emission of the three models. Each power spectrum has been smoothed in the frequency domain by a running Gaussian ($\sigma = 2.5$ Hz) to enhance the visibility of the overall features.

We recall our definition of the Fourier transform of a signal rate $R(t)$ that is sampled in N_{bins} bins of equal width $\Delta = \tau/N_{\text{bins}}$,

$$h(f_k) = \Delta \sum_{j=0}^{N_{\text{bins}}-1} R(t_j) e^{i2\pi t_j k \delta f}. \quad (3)$$

The frequencies are $f_k = k/\tau = k\delta f$ with $k = 0, \dots, N_f$ and $N_f = f_{\text{max}}/\delta f$. Here $f_{\text{max}} = 1/2\Delta$ is the Nyquist frequency. Since $\delta f = 1/\tau$ we have $N_f = N_{\text{bins}}/2$. We give the values for the frequency resolution δf for our three cases in Table I. We use $\Delta = 1$ ms, providing a Nyquist frequency of $f_{\text{max}} = 500$ Hz as an upper cutoff¹. The spectral power, a dimensionless number, is

$$P(f_k) = 2 \frac{|h(f_k)|^2}{N_{\text{bins}}^2} \quad (4)$$

except for $f = 0$ and f_{max} where the factor of 2 drops out.

We use a Hann window function to suppress edge effects. Note that our power spectrum is in absolute units, not relative to the average signal. The Fourier amplitude at $f = 0$ is the average rate per bin: $N_{\text{events}}/N_{\text{bins}}$. The power at $f = 0$ is therefore $P_0 = (N_{\text{events}}/N_{\text{bins}})^2$, which fixes the overall normalization and is given for our three cases in Table I.

Returning to Fig. 2, the logarithmic panels show the familiar fall off at high frequencies previously seen in Figs. 5 and 6 of Ref. [6]. This decrease is caused by the spatial integration over the entire visible hemisphere of the “boiling” stellar matter. The linear panels show significant peaks at familiar frequency values. In the L15 model, we see a wide double peak at 25–50 Hz and a broad bump stretching roughly from 60 to 85 Hz, as well as a few peaks at higher frequencies. Model W15 displays a clear peak at 55 Hz, along with peaks at 80 Hz and ~ 112 Hz. A significant peak around 55 Hz is also visible in N20, but this time it is accompanied by an even larger peak at 30 Hz. Further strong peaks are visible at 90 and 110 Hz, and two weaker ones at 75 and 125 Hz.

The frequencies of the peaks in the power spectra are similar to those that we found in our previous analysis of 2D models [6]. This is remarkable because the dynamics of the postshock layer and the morphology of the accretion flow in the 3D simulations appear to be considerably different from those observed in 2D calculations. While the 2D dynamics is strongly influenced by violent, large-amplitude SASI sloshing motions along the symmetry axis, such a phenomenon is not visible in the 3D runs. The much larger amplitudes of the neutrino-emission variations in 2D imply that the SASI sloshing

¹ Our chosen 1 ms binning is more convenient than IceCube’s native 1.64 ms bin width. The only change is a slightly increased Nyquist frequency which is inconsequential for our discussion

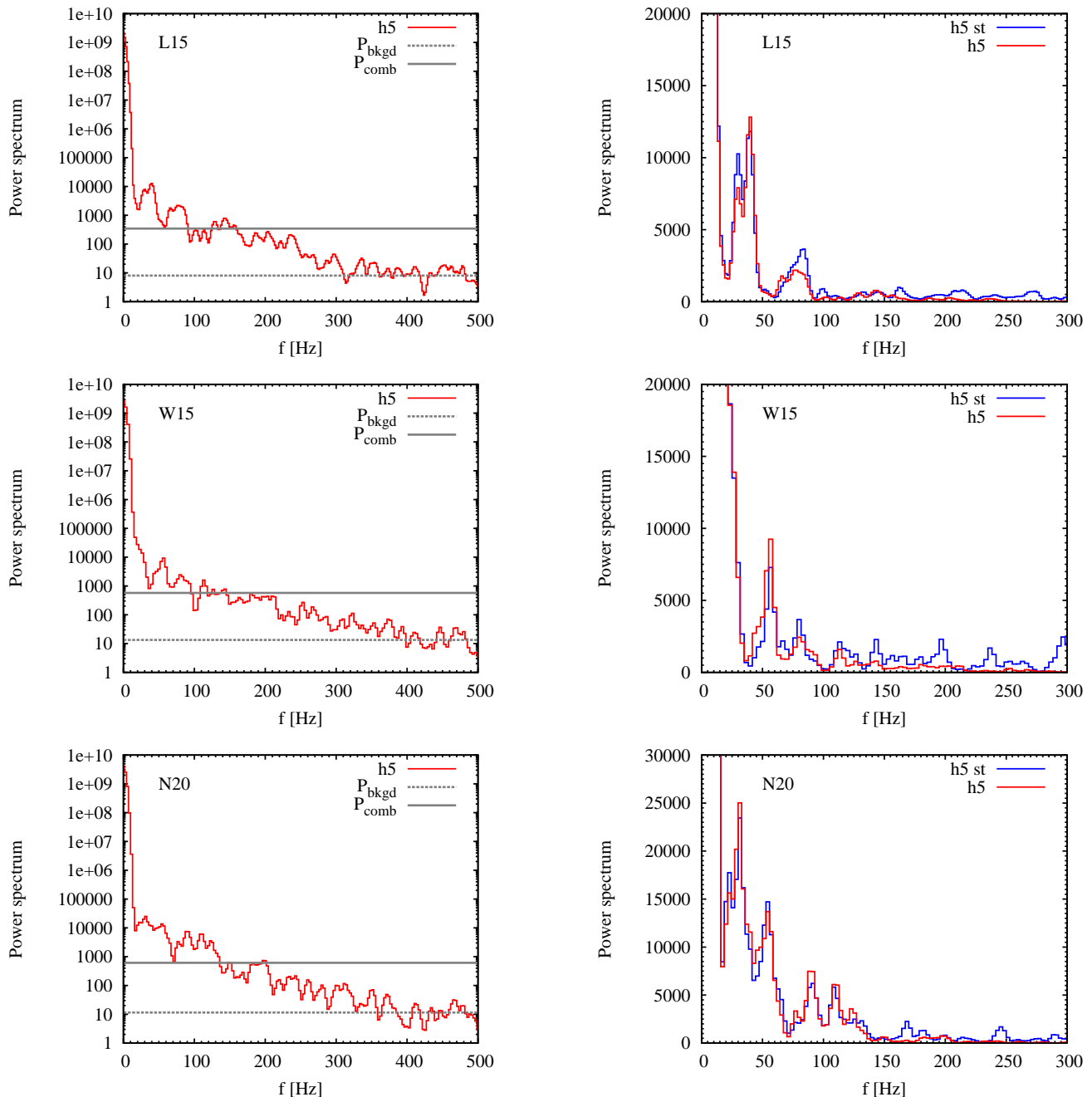


FIG. 2. (color online). Power spectra for our three models as indicated, in each case for hemisphere 5 and a distance of 1 kpc. We also show the average power levels for the shot noise arising from the IceCube dark current (P_{bkgd} , dashed gray line) and from the average signal plus background fluctuations (P_{comb} , solid gray line). The right panels use a linear scale and in addition show sample realizations (blue) where shot noise has been included.

motions are able to enhance the luminosity and energy fluctuations. A strong effect is fostered by the large spatial coherence scale of the 2D flow pattern, which channels accreted matter alternately toward the north and south polar regions [5]. The similarity of the peak frequencies, however, suggests that in 2D as well as in 3D the modulation of the hot spots of neutrino emission is governed by the same basic effect, namely the tempo-

ral coherence of the asymmetric accretion pattern, which is linked to the timescale of mass advection from the shock to the PNS surface (see Sect. II B). For similar shock and NS radii and similar advection velocities, the emission variability occurs on comparable characteristic timescales. In this context the slightly lower frequency of the first peak in models L15 and N20 (around 30 Hz) compared to model W15 (near 50 Hz) can be explained by

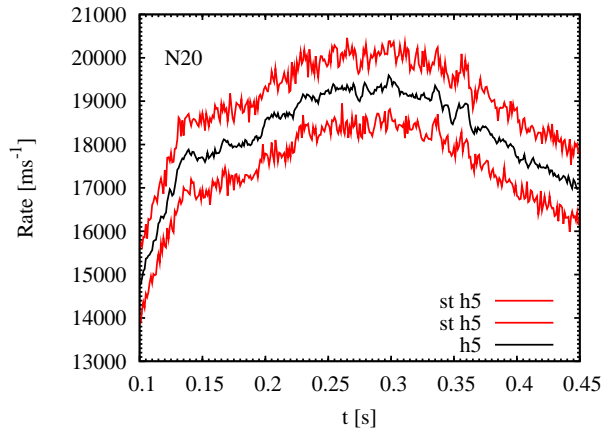


FIG. 3. (color online). Event rate for a SN at 2 kpc, including IceCube dark current. The black line is the signal for the N20 model, the red lines are two realizations when shot noise is added (curves are offset by ± 800 units).

the smaller shock stagnation radius in the W15 case [20].

Although these arguments appear plausible, a satisfactory theoretical understanding of the peaks in the power spectra is still lacking. The sequence of peaks might point to the existence of a fundamental frequency and higher harmonics, but the underlying reason is unclear. Moreover, a detailed comparison of dimension-dependent effects will require 2D and 3D modeling with the same level of sophistication instead of the approximations used in the present set of 3D runs as described in Sect. II A.

IV. DETECTABILITY

The detectability of features in the power spectrum depends on their significance relative to random fluctuations (shot noise). In Fig. 3 we show an example of a SN signal at 2 kpc without shot noise (black line) and two realizations with shot noise added, each time using our usual 1 ms bins. Visually the shot noise competes with the intrinsic signal variations and indeed a distance of 2 kpc is about the limiting case where signal variations can still be detected. The probability of a future galactic core collapse SN being within 2 kpc of Earth is only a few percent of the total galactic rate [37] of a few per century. Therefore, the prior probability of such an event is, of course, very small, yet not completely excluded.

As explained in our previous paper [6], the average of the shot noise provides a flat power spectrum. In the framework of our definitions, and using a Hann window function, the power-level of the shot noise is

$$P_{\text{shot}} = 3N_{\text{events}}/N_{\text{bins}}^2. \quad (5)$$

Here N_{events} is the total number of events in the analysis interval of duration τ .

One unavoidable source of shot noise is the IceCube dark current with the rate R_{bkgd} , providing the shot noise

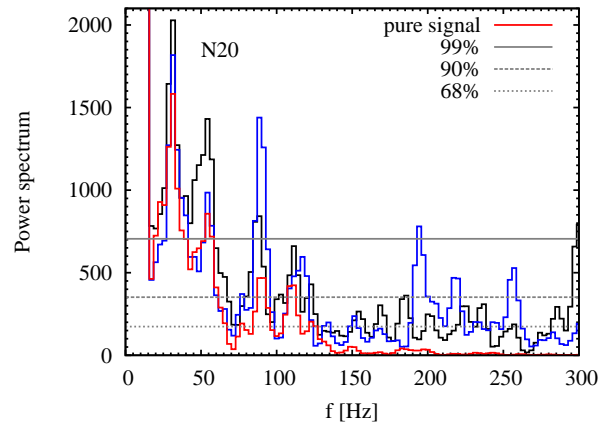


FIG. 4. (color online). Power spectrum for the signal from hemisphere 5 of the N20 model, for a SN at 2 kpc (red line) and two realizations with added statistical noise (blue and black lines). The 99%, 90% and 68% levels are also shown (grey lines).

level P_{bkgd} shown for our three cases in Table I. The signal variations in our models are now so weak that we need a relatively close SN to detect these variations, which in turn means that the SN signal contributes much more to the counting rate than the dark current. Therefore, the dominant source of shot noise is now the signal itself and we give the corresponding power levels in Table I as P_{comb} which includes the combined shot noise from the signal itself and the dark current. We also show the average power levels P_{bkgd} and P_{comb} in the left panels of Fig. 2. It is immediately obvious that even at 1 kpc one cannot hope to detect significant signal power at frequencies exceeding some 150 Hz.

The same point can be made by the right panels of Fig. 2 where we show the power spectra on a linear scale, together with typical realizations including shot noise for a SN at 1 kpc. For the signal with added shot noise the power spectrum clearly retains the intrinsic low frequency peaks. In addition, relatively strong peaks appear for frequencies $f \gtrsim 150$ Hz.

To evaluate how likely it is that a peak caused by fluctuations mimics a real peak, we calculate the power level where 99% of random peaks should lie below. From the expressions given in our previous paper we find these limiting power levels P_{99} and give them in Table I. In Fig. 4 we show a pure signal (red line) and two signals with addition of different shot noise realizations (black and blue curves). The grey lines give the levels where 99%, 90% and 68% of the purely random peaks should lie below. We see that the main peaks at $f \sim 30$ Hz, 50 Hz, and 90 Hz can all be identified.

The power of the shot noise relative to the signal scales linearly with distance, i.e. at twice the distance, the shot noise is twice larger relative to the signal power. We conclude that at distances exceeding 2 kpc it will be nearly impossible to distinguish intrinsic signal variations from

random fluctuations caused by the limited counting rate.

V. SUMMARY AND CONCLUSIONS

We have shown that also for 3D SN models time variations of the neutrino emission lead to distinct peaks in the power spectra as previously seen for 2D results [6]. Despite considerably smaller amplitudes of the luminosity and mean energy fluctuations than in the 2D simulations, these features will still be detectable in the IceCube event rate for a future galactic SN within 2 kpc distance. Up to frequencies of about 150 Hz such features will hint to intrinsic flux variations, whereas above this frequency they will, with a high probability, be associated to statistical effects in the measurement of the signal.

A thorough discussion is hampered by the simplifications made in the 3D models and the small set of investigated cases. In particular, the neutrino signals evaluated in this work are based on an approximate grey treatment of the neutrino transport in models, in which the high-density core of the PNS was excised and replaced by a boundary condition. Nevertheless, the signals exhibit all familiar features also predicted by more sophisticated transport schemes in fully self-consistent 1D and 2D simulations. The largest emission variations are observed during the postbounce accretion phase until shortly after shock revival, when the SN core is stirred by violent hydrodynamical instabilities. Large-scale asymmetries and intermittent behavior characterize the accretion flows to the nascent NS during this phase. Interestingly, the power spectra of the 3D models show similar peaks in the same frequency range as those found in 2D, although the flow dynamics in 3D appears to be largely different. In particular, the strong SASI sloshing motions that are constrained to the symmetry axis in the 2D case and that are responsible for big emission variations, cannot be seen prominently in the 3D simulations.

If the existence of the frequency peaks is consolidated by better 3D models, these features will offer a powerful diagnostic for the dynamics in the SN core and the explosion mechanism. The role of turbulence and violent nonradial mass motions in the postshock layer during the accretion phase and on the way to shock revival is presently a matter of vivid debate [12, 22, 23]. A better understanding of the characteristic imprints of the SASI and of convective overturn motions on the neutrino emission in 3D is therefore desirable.

Our previously investigated 2D models together with the 3D simulations analyzed in this work can be considered to span the range between optimistic and pessimistic cases with respect to the possible level of signal variability. It is not excluded that fully self-consistent 3D models will reveal higher fluctuation amplitudes of the neutrino emission. Stronger SASI activity and especially the development of spiral modes [38], whose growth could be fostered by even a relatively small amount of rotation in the SN core, can not be excluded on grounds of the small set of presently available 3D simulations.

ACKNOWLEDGMENTS

We thank the Institute for Nuclear Theory at the University of Washington for its hospitality and the Department of Energy for partial support while this work was completed during the INT Program INT 12-2a “Core-Collapse Supernovae: Models and Observable Signals”. In Munich and Garching, we acknowledge partial support by the Deutsche Forschungsgemeinschaft under grant TR-7 “Gravitational Wave Astronomy” and the Cluster of Excellence EXC-153 “Origin and Structure of the Universe.” T.L. acknowledges support from the MPA in Garching and the MPP in Munich, as well as hospitality at Aarhus University, while much of this work was done.

-
- [1] H. A. Bethe and J. R. Wilson *Astrophys. J.* **295**, 14 (1985).
 - [2] H.-Th. Janka, Accepted by *Annual Rev. of Nuclear and Particle Science* [arXiv:1206.2503v1].
 - [3] H. A. Bethe, *Rev. Mod. Phys.* **62**, 801 (1990).
 - [4] J. M. Blondin, A. Mezzacappa and C. DeMarino, *Astrophys. J.* **584**, 971 (2003) [astro-ph/0210634].
 - [5] A. Marek, H.-Th. Janka and E. Müller, *Astron. Astrophys.* **496**, 475 (2009) [arXiv:0808.4136].
 - [6] T. Lund, A. Marek, C. Lunardini, H.-Th. Janka and G. G. Raffelt, *Phys. Rev. D* **82**, 063007 (2010) [arXiv:1006.1889].
 - [7] T. D. Brandt, A. Burrows, C. D. Ott and E. Livne, *Astrophys. J.* **728**, 8 (2011) [arXiv:1009.4654].
 - [8] J. Ellis, H.-Th. Janka, N. E. Mavromatos, A. S. Sakharov and E. K. G. Sarkisyan, *Phys. Rev. D* **85**, 105028 (2012) [arXiv:1202.0248].
 - [9] J. Ellis, H.-Th. Janka, N. E. Mavromatos, A. S. Sakharov and E. K. G. Sarkisyan, *Phys. Rev. D* **85**, 045032 (2012) [arXiv:1110.4848].
 - [10] A. Marek and H.-Th. Janka, *Astrophys. J.* **694**, 664 (2009) [arXiv:0708.3372].
 - [11] B. Müller, H.-Th. Janka and A. Marek, Accepted by *Astrophys. J.* (2012) [arXiv:1202.0815].
 - [12] B. Müller, H.-Th. Janka and A. Heger, arXiv:1205.7078.
 - [13] Y. Suwa, K. Kotake, T. Takiwaki, S. C. Whitehouse, M. Liebendörfer and K. Sato, *Publ. Astron. Soc. Japan* **62**, L49 (2010) [arXiv:0912.1157].
 - [14] J. W. Murphy and A. Burrows, *Astrophys. J.* **688**, 1159 (2008) [arXiv:0805.3345].
 - [15] J. Nordhaus, A. Burrows, A. Almgren and J. Bell, *Astrophys. J.* **720** 694 (2010) [arXiv:1006.3792].
 - [16] F. Hanke, A. Marek, B. Müller and H.-Th. Janka, Accepted by *Astrophys. J.* (2012) [arXiv:1108.4355].

- [17] J. M. Blondin and A. Mezzacappa, *Astrophys. J.* **642**, 401 (2006) [astro-ph/0507181].
- [18] W. Iwakami, K. Kotake, N. Ohnishi, S. Yamada and K. Sawada, *Astrophys. J.* **678**, 1207 (2008) [arXiv:0710.2191].
- [19] A. Wongwathanarat, H.-Th. Janka and E. Müller, *Astrophys. J.* **725**, L106 (2010) [arXiv:1010.0167].
- [20] E. Müller, H.-Th. Janka and A. Wongwathanarat, *Astron. Astrophys.* **537**, A63 (2012) [arXiv:1106.6301].
- [21] T. Takiwaki, K. Kotake and Y. Suwa, *Astrophys. J.* **749**, 98 (2012) [arXiv:1108.3989].
- [22] A. Burrows, J. C. Dolence and J. W. Murphy, arXiv:1204.3088.
- [23] J. W. Murphy, J. C. Dolence and A. Burrows, arXiv:1205.3491.
- [24] W. Iwakami, K. Kotake, N. Ohnishi, S. Yamada and K. Sawada, *Astrophys. J.* **700**, 232 (2009) [arXiv:0811.0651].
- [25] R. Fernández, *Astrophys. J.* **725**, 1563 (2010) [arXiv:1003.1730].
- [26] T. Yamasaki and T. Foglizzo, *Astrophys. J.* **679**, 607 (2008) [arXiv:0710.3041].
- [27] T. Foglizzo, F. Masset, J. Guilet and G. Durand, *Phys. Rev. L.* **108**, 051103 (2012) [arXiv:1112.3448].
- [28] S. E. Woosley and T. A. Weaver *Astrophys. J. Suppl.* **101**, 181 (1995).
- [29] M. Limongi, O. Straniero and A. Chieffi, *Astrophys. J. Suppl.* **129**, 625 (2000) [arXiv:astro-ph/0003401].
- [30] T. Shigeyama and K. Nomoto, *Astrophys. J.* **360**, 242 (1990).
- [31] B. Fryxell, E. Müller and D. Arnett, *Astrophys. J.* **367**, 619 (1991).
- [32] E. Müller, B. Fryxell and D. Arnett, *Astron. Astrophys.* **251**, 505 (1991).
- [33] E. Müller, B. Fryxell and D. Arnett, in *European Southern Observatory Conference and Workshop Proceedings*, Vol. 37, ed. I. J. Danziger and K. Kjaer, 99 (1991).
- [34] A. Kageyama and T. Sato, *Geochemistry Geophysics Geosystems* **5** Q09005 (2004) [arXiv:physics/0403123].
- [35] A. Wongwathanarat, N. J. Hammer and E. Müller, *Astron. Astrophys.* **514**, A48 (2010).
- [36] L. Scheck, K. Kifonidis, H.-Th. Janka and E. Müller, *Astron. Astrophys.* **457**, 963 (2006).
- [37] A. Mirizzi, G. G. Raffelt and P. D. Serpico, *JCAP* **0605**, 012 (2006) [astro-ph/0604300].
- [38] J. M. Blondin and A. Mezzacappa, *Nature* **445**, 58 (2007) [arXiv:astro-ph/0611680].